Al-Mustansiriyah Journal of Science
ISSN: 1814-635X (print), ISSN: 2521-3520 (online)
Volume 29, Issue 3, 2018
DOI: http://doi.org/10.23851/mjs.v29i3.636

**Research Article** **Open Access**

# Enhanced Ultraviolet Photodetector Based on Mg-Doped ZnO Nanorods Films

**Hussein Abdullah Hameed[1, 2*], J. J. Hassan[2], H. L. Saadon[2]**
[1]*Department of Physics, Faculty of Science, University of Kufa, IRAQ*
[2]*Department of Physics, Faculty of Science, University of Basrah, IRAQ*
**Correspondent author email: husseina.alshemirti@uokufa.edu.iq*

**ArticleInfo**

Received
02/10/2018

Accepted
20/10/2018

Published
10/03/2019

## Abstract

Magnesium-doped zinc oxide (ZnO: Mg) nanorods and nanotubes films were prepared by hydrothermal method deposited on glass substrates. X-ray diffraction (XRD), scanning electron microscopy (SEM), energy-dispersive X-ray spectroscopy (EDX), photoluminescence (PL), and optical absorption spectroscopy (UV) were performed to characterize the prepared films. X-ray diffraction analysis showed a decrease in the lattice parameters of Mg doped ZnO NRs. The Photoluminescence of the undoped and Mg-doped ZnO NRs displayed a near band edge. At 10 V bias, the metal-semiconductor-metal (MSM) ultraviolet (UV) photodetector performance of the Mg-doped ZnO prepared for various Mg concentrations of 0.0, 0.02, and 0.06 was investigated under radiation of 40μW/cm$^2$ at the wavelengths of 365 and 385 nm UV light. The responsivity, detectivity and quantum efficiency of Mg-doped based on MSM detector were 0.118A/W, 1.0579*10$^{12}$ and 40.05157 under UV of wavelength 365nm respectively.

**Keywords:** pure ZnO nanorods Mg doping ZnO nanorods, MSM Photodetector, hydrothermal method, nanotubes.

## الخلاصة

تم تحضير اغشية أوكسيد الزنك النقي والمشوب بالمغنيسيوم بتراكيز مختلفة على قواعد زجاجية بالطريقة الحرارية المائية . تم اجراء فحوصات حيود الأشعة السينية (XRD) ، المسح المجهري الإلكتروني (SEM) ، (EDX)، (PL)، (UV) لتوصيف واختبار الاغشية المحضرة. أظهرت تحليلات حيود الأشعة السينية (XRD)بان جميع النماذج متعددة البلورات ذات تركيب سداسي بالاتجاه (٠٠٢). تم دراسة تأثير تشويب المغنيسيوم على الخصائص التركيبية والكهربائية والبصرية لأغشية اوكسيد الزنك ZnO، ولوحظ التحسن الواضح على التبلور وكذلك زيادة في فجوة الطاقة البصرية. عند تحيز ١٠ V ، تم فحص أداء كاشف (MSM) للزنك اوكسايد النقي والمشوب بالمغنيسيوم بتراكيز مختلفة من ٠,٠ و ٠,٠٢ و ٠,٠٦ تحت اشعة الفوق البنفسجية ذات شدة ٤٠ μ واط / سم ٢ عند أطوال موجية ٣٦٥ و ٣٨٥ نانومتر . كانت الاستجابة والكشفية والكفاءة الكمية لكاشف الزنك المشوب بالمغنيسيوم بتركيز 0.06, ٠,١١٨ A / W , ١,٠٥٧٩ *10$^{12}$ و ٤٠,٠٥١٥٧ عند الطول الموجي ٣٦٥ nm للأشعة الفوق البنفسجية على التوالي.

## Introduction

Zinc oxide is a semiconductor material composed of zinc ions ($Zn^{2+}$) and oxygen ions ($O_2$), represented by ZnO. It has special electrical, optical and electrical properties. It also has a large energy gap and a relatively large exciton binding energy of about 3.37eV and 60 MeV respectively and with room temperature [1, 2]. Different doping in ZnO (i.e., Mg) can adjust bandgap to make UV photodetectors in different UV region. There were several reports focused on efforts to control the properties of ZnO by adding the transition metal impurities such as Al [3, 4], Cu [5], Co [6], In [7], and Mg [3, 8] Doping work to control and adjust the band gap, which greatly contribute to increase the efficiency and power, and in many applications, such as Light-emitting diodes [9], laser diodes

[10], solar cells, transparent electrodes, thin film transistors and optical sensors [3, 11].

The ZnO sensing mechanism is highly correlated with surface reactions hence; oxygen absorption, grain size, defects, and other parameters have an important effect in controlling the sensing response.

In the present study, systematic Mg doping (0, 0.02, 0.06) in ZnO NPs was achieved and is analyzed by XRD, SEM, and UV-Vis spectroscopy and it has discussed the fabrication of Metal Semiconductor Metal (MSM) UV photodetector that importance of this study is the amplification of (MSM) UV detectors performance using ZnO nanorods arrays, resulting in a low-cost, time-saving fabrication process. It has also discussed the performance of (MSM) UV detectors fabricated using Mg-doped ZnO nanorods and nanotubes that produce the highest responsivity, quantum efficiency and others parameters compared with pure ZnO.

## Materials and Methods

### *Experimental*

The hydrothermal method was used to synthesize pure and Mg-doped ZnO nanorods and nanotubes arrays as reported by several researchers [3, 12]. First, ultrasonic cleaner technology was used to clean the glass substrates in stages, starting with ethanol, acetone, and propanol for 10 minutes per solvent, then cleaning with deionized water and drying it.

Zinc acetate dehydrates 0.5 M was first dissolved in the ethanol with stirring at 60C° for (2-3) h until a clear and transparent homogeneous solution was formed. A homogeneous seed layer was obtained using a spin coating technique by taken by dropper of the prepared solution and pours over the center of a substrate, the rate of speed was 2500 for 30 seconds, this process was repeated several times on hotpot temperatures about (140-150) C° for 10 min per cycle to remove the solvent, then the samples were finally annealed at (350-400) C° in the furnace for 2 h to getting the ZnO seed layer.

After the formation of a seed layer, ZnO nanorods were formed through the hydrothermal method. The substrates with a seed layer were putting verticality inside Teflon vessels filled with the aqueous solution of 0.05M zinc nitrate hexahydrate $Zn(NO_3)_2 \cdot 6H_2O$) and 0.05 M Hexamethylenetetramine $C_6H_{12}N_4$, sealed and heated at (110-120) C° for 3 h. Then, the substrate removed from the Teflon vessel, cleaned with distilled $H_2O$ and dried. Next, the Mg-doped ZnO nanorods and nanotubes were grown on the seed-layer-coated glass substrate using aqueous solutions of 0.05M zinc nitrate hexahydrate, 0.05M Hexamethylenetetramine and concentrations (the atoms' ratio of Mg to Zn) Mg/Zn (0.02, 0.06) magnesium nitrate $Mg(NO_3)_2 \cdot 6H_2O$. These reagents were dissolved and reacted in Teflon vessel with a temperature of (110-120) C° for 3h.

Following, the substrate was rinsed with distilled water and all the samples were annealed for 2h in furans at 350C°. Then aluminum Al contacts were deposited on the nanorods or nanotubes films by using a thermal evaporator technique to produce a metal–semiconductor–metal (MSM)-type UV photoconductive detector. The deposition of metal contacts was performed at a low pressure of $9.5 \times 10^{-5}$ Pa. The separation between the metal contacts was fixed at 0.05 mm for all samples using a metal mask as showed in Table1.

Table 1: Represent as name and ratio Mg-doped ZnO for samples used in this paper

| samples | element | ratio atoms Mg/ atoms Zn doped ZnO |
|---|---|---|
| **A** | pure ZnO | 0 |
| **M1** | Mg | 0.02 |
| **M2** | Mg | 0.06 |

## Results and discussions

### *Structural studies*

Pure and Mg-doped ZnO nanorods and nanotubes have a polycrystalline hexagonal wurtzite structures as shown in Figure1, it is noted that the intensity of diffraction peaks of the ZnO deposition appears at positions 31.2954,

34.44, 35.9651, 47.87, 56.85 and 63.1 which correspond to the (1 0 0), (0 0 2), (1 0 1), (1 0 2), (1 1 0) and (1 0 3) orientations respectively. The peak positions of all samples corresponding to ZnO according to the standard JCPDS card with hexagonal wurtzite structure [13]. The intensity diffraction peaks (1 0 0), (0 0 2) and (1 0 1) orientations for the Mg-doped ZnO prepared at different Mg concentrations M1 (0.02) and M2 (0.06) deposited on the glass substrate, appear at positions 31.583, 34.495 and 36.037 and 31.665, 34.521 and 36.157 respectively, [2, 13], this shift in the (1 0 0, 0 0 2, 1 0 1) peaks for Mg-doped ZnO might be due to the substitution of Zn by Mg in the hexagonal lattice. The position peaks shift agree with previous reports [2, 3], where any change in the crystalline structure was detected when adding impurities. The interplanar spacing, the lattice constant (a, c) and the micro-strain ( $\varepsilon$ ) can be found by the equations (1-3).

$$2d\sin\theta = n\lambda \tag{1}$$

$$\frac{1}{d^2} = \frac{4(h^2 + hk + k^2)}{3a^2} + \frac{l^2}{c^2} \tag{2}$$

$$\varepsilon = \frac{\beta\cos\theta}{4} \tag{3}$$

where *h*, *k* and *l* are miller indices, as given in Table2.

Table 2: The crystalline size, interplanar spacing, lattice… synthesized for the all samples

| sample | h k l | $2\theta^\circ$ | d (A°) | a, c (A°) | $\varepsilon$ |
|---|---|---|---|---|---|
| A | 1 0 0 | 31.2954 | 2.85621 | 3.29806, | 0.05686 |
| | 0 0 2 | 34.44 | 2.60227 | 5.20453 | 0.0282 |
| | 1 0 1 | 35.9651 | 2.49533 | | 0.0234 |
| M1 | 1 0 0 | 31.583 | 2.83085 | 3.26878, | 0.07458 |
| | 0 0 2 | 34.495 | 2.59824 | 5.19649 | 0.05969 |
| | 1 0 1 | 36.037 | 2.49052 | | 0.11745 |
| M2 | 1 0 0 | 31.665 | 2.82371 | 3.26054, | 0.07817 |
| | 0 0 2 | 34.521 | 2.59635 | 5.19269 | 0.08476 |
| | 1 0 1 | 36.157 | 2.48253 | | 0.09697 |

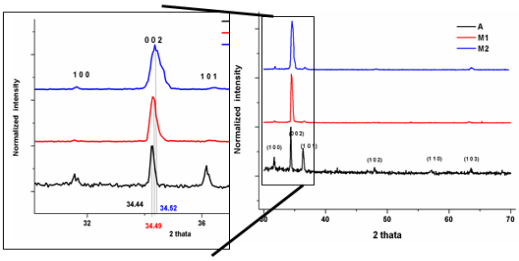


Figure 1: XRD patterns for pure ZnO and Mg-doped ZnO nanorods/nanotubes deposited on the glass substrate

### *FESEM and EDX Analysis*

The surface morphology of the grown pure and Mg-doped ZnO nanorods and nanotubes (A and M2) was investigated by the Field-Emission Scanning Electron Microscope (FESEM). The results can be shown in Figure2 with hexagonal rod shapes at diameters ranging from 60- 80 nm. The chemical composition at different concentrations (the atoms ratio of Mg to Zn) Mg/Zn 0, 0.02, and 0.06 (A, M1, and M2) were measured by using EDX shown as in Figure3.

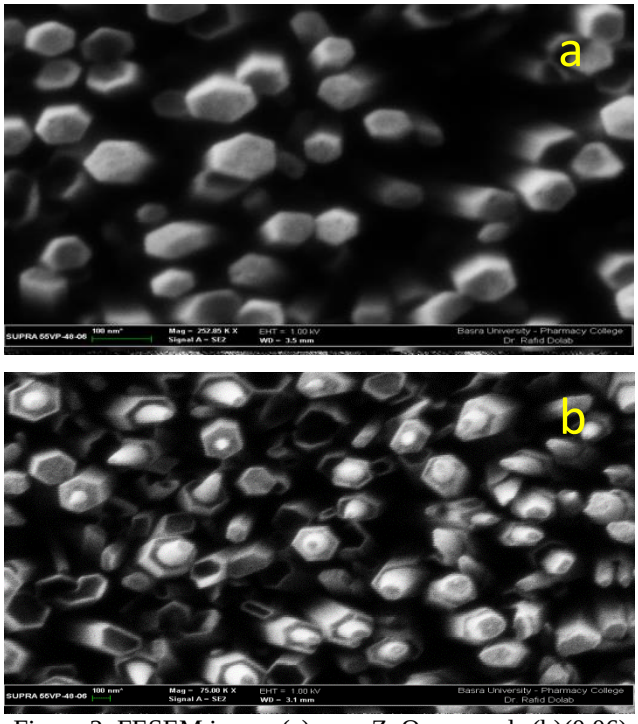


Figure 2: FESEM image (a) pure ZnO nanorods (b)(0.06) Mg-doped ZnO nanorods and nanotubes

Spectrum: Acquisition

| Element | Series | unn. C [wt.%] | norm. C [wt.%] | Atom. C [at.%] | Error (1 Sigma) [wt.%] |
|---|---|---|---|---|---|
| Zinc | L-series | 72.94 | 75.20 | 42.60 | 4.69 |
| Oxygen | K-series | 24.05 | 24.80 | 57.40 | 4.06 |
| | Total: | 97.00 | 100.00 | 100.00 | |

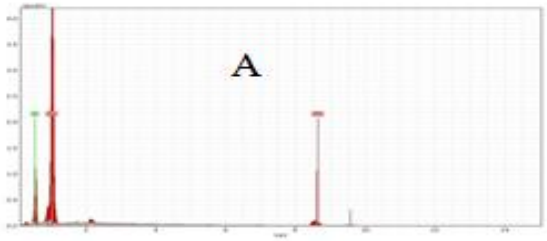


Spectrum: Acquisition

| Element | Series | unn. C [wt.%] | norm. C [wt.%] | Atom. C [at.%] | Error (1 Sigma) [wt.%] |
|---|---|---|---|---|---|
| Oxygen | K-series | 20.98 | 26.41 | 59.09 | 3.05 |
| Zinc | L-series | 57.90 | 72.90 | 39.90 | 3.69 |
| Magnesium | K-series | 0.55 | 0.69 | 1.02 | 0.07 |
| | Total: | 79.43 | 100.00 | 100.00 | |

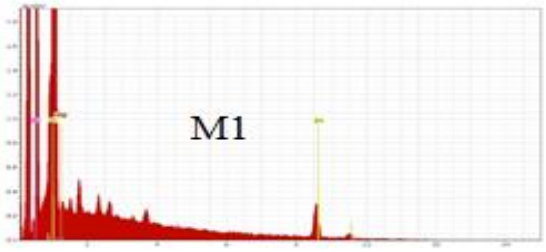


Spectrum: Acquisition

| Element | Series | unn. C [wt.%] | norm. C [wt.%] | Atom. C [at.%] | Error (1 Sigma) [wt.%] |
|---|---|---|---|---|---|
| Oxygen | K-series | 22.53 | 28.50 | 61.32 | 8.03 |
| Zinc | L-series | 55.61 | 70.35 | 37.04 | 4.46 |
| Magnesium | K-series | 0.92 | 1.16 | 1.64 | 0.29 |
| | Total: | 79.06 | 100.00 | 100.00 | |

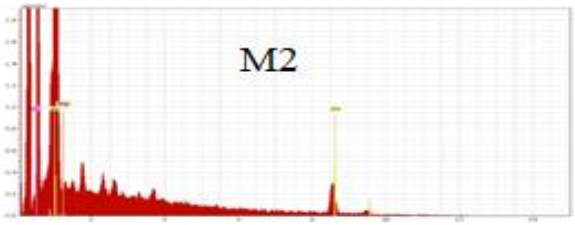


Figure 3: EDX spectrum of ZnO and Mg-doped ZnO (A, M1 and M2)

***Optical properties***

The optical absorption spectrum of undoped and Mg-doped ZnO nanorods and nanotubes as shown in Figure4a at room temperature; it showed that all samples have sharp absorption edges in the UV region. The absorption band edge was observed at 390 nm, 382.5 nm, and 379 nm for samples A, M1, and M2, respectively, because of the band-to-band transition and Mg-doped ZnO shows that the absorption edge shifted to a short wavelength with an increase in the doping ratio due to quantum-size effects. The optical bandgap of ZnO was calculated using the fundamental relation [13-15]

$$(Ah\upsilon) = B(h\upsilon - E_g)^n \qquad (4)$$

Where A, $\upsilon$, h, and $E_g$ represent the absorbance, frequency, Planck's constant and optical energy gap respectively, n =1/2 for direct allowed transition and B is the proportionality constant. The optical energy gap of the A, M1, and M2 was observed equal to 3.23, 3.275, and 3.296 eV, respectively [3] as shown in Figure4b, agreed with the theoretical band gap value of 3.37 eV. However, it was noted that with Mg doping an increasing in the energy gap of pure ZnO with a blue shift that can be attributed to that the new ion ($Mg^{+2}$) energy level formed in the energy gap, thereby increasing the ZnO band gap.[3, 16]

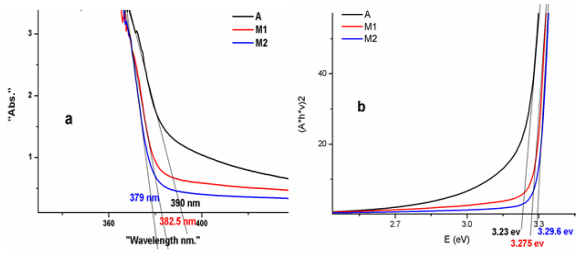


Figure 4: Absorption spectra and b) the optical energy gap of pure ZnO and Mg-doped ZnO nanorods deposited on the glass substrate

***Photoluminescence spectra***

The photoluminescence (PL) spectra for pure and Mg-doped ZnO nanorods samples with excitation at a wavelength of 325 nm show that Figure5, That is showing the photoluminescence (PL) spectra of samples A, M1 and M2 at peaks 389.8, 382.5 and 378.3 nm at sharp UV emission due to the recombination of free-exciton across which was called the near band edge emission (NBE). A minor broad visible emission, which is called deep level emission (DLE) that range of wavelength 450–550 nm [3, 17], due to the transition between defect levels as well as extrinsic impurities [18]. The near band edge emission (NBE) of samples A, M1 and M2 were detected at UV peaks 387.8, 381.66, and 377.45 respectively with excitation a wavelength of 325 nm. The increase in the Mg composition of the samples leading to widening of the bandgap and blue shifted the NBE emission. [19]. Thus, Mg doping should be responsible for such a blue shifted. PL spectra showed an increase in DLE upon doping which was due to the increase in defect states [20], the effect of oxygen may be one of the defects in the composition of materials according to researches [3, 21] and shows its obvious effect in Figure5, the defect green emission occurred around 543nm, 541nm and 538nm for samples A, M1 and M2 respectively, which was due to the presence of $O_i$ according to the previous reports by [22].

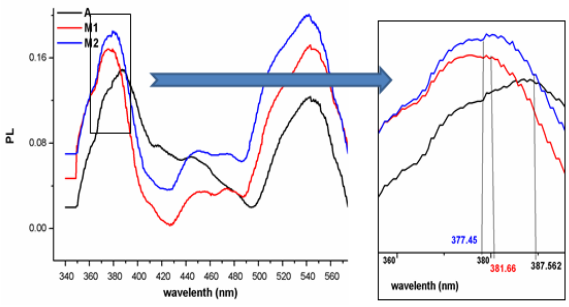


Figure 5: PL spectra of undoped ZnO and Mg doped ZnO nanotubes and nanorods with concentration M1 and M2 deposited on the glass substrate

## Device Fabrication Process

The UV photodetector device with a dimension of 1 cm x 1 cm for the structure of Al/ZnO/Al was fabricated by the MSM. The Al electrode was deposited onto samples A, M1, M2 and the annealed films using a mask through thermal evaporation technique.

***Characteristic of the UV detector***

The current-voltage (I-V) curves of the fabricated MSM under dark and UV (365, 385) nm with power density of 40μW/cm$^2$ were measured for all samples. The results can be shown in Figure6; it showed a linear response of the photocurrent density curve; that can be attributed to an ohmic contact between the ZnO film and Al electrodes. The highest sensitivity or higher ratio between the electrical resistance under the action of light and the dark state can be obtained when the conductivity between the metal and the ZnO is a ohmic connection [3, 23]. The responsivity (R), quantum efficiency ($\eta$), detectivity (D) and photosensitivity (S) can be calculated by the Equations (5 to 8):

$$R = \frac{I_{ph} - I_{dark}}{P_{opt}} \quad (5)$$

$$\eta = R\frac{hc}{e\lambda} \quad (6)$$

$$D = \frac{\lambda\eta e}{hc}\left(\frac{RA}{4kT}\right)^{1/2} \quad (7)$$

$$S = \frac{I_{ph} - I_{dark}}{I_{dark}} * 100\% \quad (8)$$

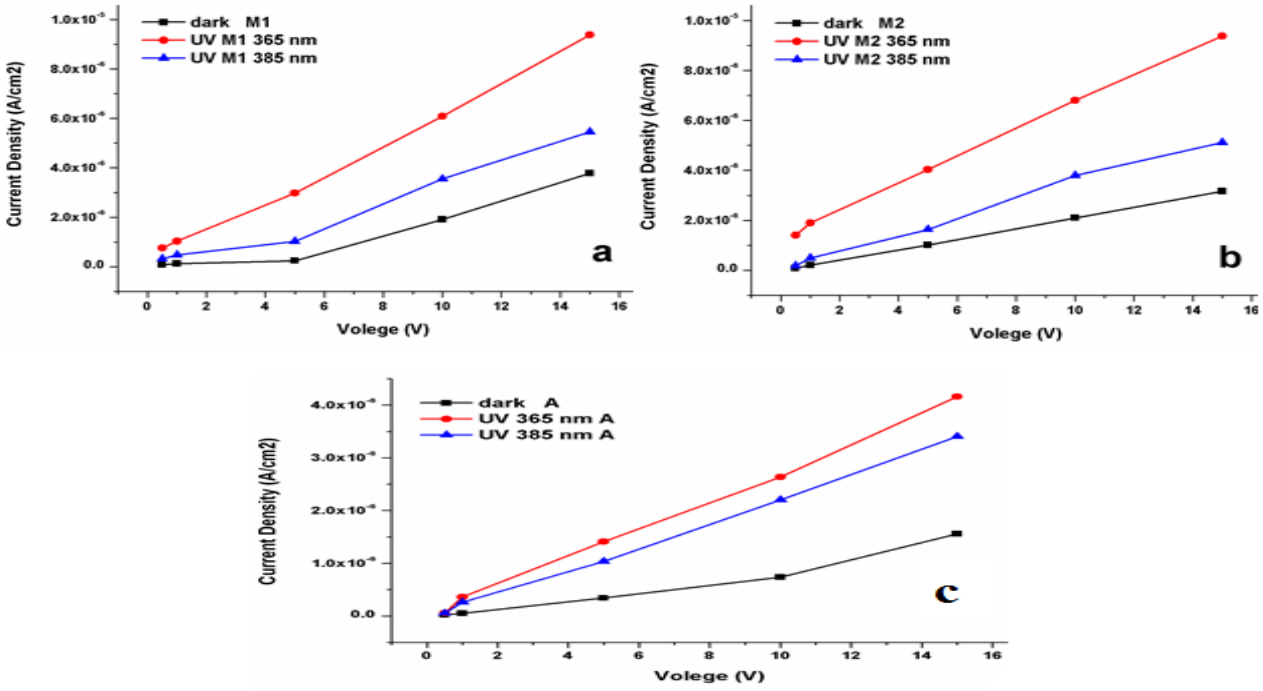


Figure 6: I–V characteristics for MSM ZnO and Mg-doped ZnO in dark and under Uv 365 and 385 nm for samples a) M1 (0.02) b) M2 (0.06) c) A (0%)

Where $I_{ph}$ is the photocurrent, $I_{dark}$ is the dark current and $P_{opt}$ is the optical power of the UV source, c, e and $\lambda$ are represented blank constant, light speed, electron charge and wavelength used, respectively. According to the relations (5-8), the results can be found in Table3, at a wavelength of 365, 385 nm is as a function applied voltage.

Table 3: Parameters of MSM ZnO and Mg doped ZnO photodetector as a voltage of at UV wavelength 365 nm and 385 nm

| Par. | V | 365 nm | | |
|---|---|---|---|---|
| | | A | M1 | M2 |
| $\eta$ | 1 | 2.6242 | 7.74393 | 14.3516 |
| | 5 | 9.10533 | 23.30504 | 25.78499 |
| | 10 | 16.19009 | 35.54741 | 40.05157 |
| S% | 1 | 617.33333 | 746.6124 | 806.73039 |
| | 5 | 314.69148 | 1132.73421 | 300.95923 |
| | 10 | 259.56383 | 218.62517 | 224.44021 |
| D | 1 | 1.42027E11 | 2.68313E11 | 3.79689E11 |
| | 5 | 4.22366E11 | 1.282E12 | 6.95082E11 |
| | 10 | 7.2337 E11 | 9.83711E11 | 1.05797E12 |
| Gain | 1 | 7.17333 | 8.46612 | 9.0673 |
| | 5 | 4.14691 | 12.32734 | 4.00959 |
| | 10 | 3.59564 | 3.18625 | 3.2444 |
| 385 nm | | | | |
| $\eta$ | 1 | 1.70336 | 2.84456 | 2.27002 |
| | 5 | 5.60443 | 6.34055 | 5.06918 |
| | 10 | 11.84292 | 13.1947 | 13.70282 |
| S% | 1 | 422.66667 | 289.27921 | 134.59379 |
| | 5 | 204.3095 | 325.067 | 62.40883 |
| | 10 | 200.2726 | 85.5972 | 80.99512 |
| D | 1 | 9.72411E10 | 1.03959E11 | 6.33468E10 |
| | 5 | 2.74216E11 | 3.67902E11 | 1.44137E11 |
| | 10 | 5.58133E11 | 3.85148E11 | 3.81796E11 |
| Gain | 1 | 5.22667 | 3.89279 | 2.34594 |
| | 5 | 3.0431 | 4.25067 | 1.62409 |
| | 10 | 3.00273 | 1.85597 | 1.80995 |

### *The photoswitching characteristic of the UV detector*

Figure7 shows the photo response of UV photodetector at a wavelength of 365 and 385 nm. The ON/OFF switching UV time duration characteristics was 2/5 min for the samples A, M1, and M2, respectively, with the intensity of 40 μ W/cm$^2$ at 10V applied bias. According to [2, 24], the photodetector sensitivity was closely related to oxygen adsorption and desorption processes. The oxygen molecules tend to absorb the free electrons at the nanorod surfaces to produce oxygenated ions adsorbents, in the case

of darkness, i.e., without ultraviolet radiation, as shown by following equation

$$O_2 + e^- \rightarrow O_2^- \quad (9)$$

Where is $O_2$, $e^-$ and $O_2^-$ represent are oxygen molecule, a free electron and O2− adsorbed oxygen ion respectively. Before UV illumination applied, a low current is generated because a barrier is created at near the surface by the adsorbed oxygen ions. When UV light is irradiated onto the nanorods or nanotubes, an electron–hole pairs are generated at the surface according to the equation: [25]

$$h\nu \rightarrow h^+ + e^- \quad (10)$$

where $h\nu$ , $h^+$ and $e^-$ are represented the photon energy of UV light, generated hole in the valence band and generated electron in the conduction band respectively.

The $O_2$ molecules which desorbs from the surface are produced by adsorbed oxygen ions combine with the holes under applied a bias voltage, the unpaired electrons are collected at the anode; thereby an increase in conductivity takes place with the decrease in the width of the depletion layer, this process is given by the equation:

$$O_2^- + h^+ \rightarrow O_2 \quad (11)$$

At the same time, desorption of $O_2^-$ ions on the nanorods surface leaves photo generated electrons in the conduction band, increasing ZnO conductivity and contributing to the photocurrent [25, 26]. After the UV exposure, the $O_2$ molecules get reabsorbed on the surface until equilibrium is restored to repeat the process again onto the nanorod surface, making decrease the conductivity of the sensor. When the nanorods or and nanotubes array, the surface area increases, enabling UV light to be absorbed more effectively and to generate more electron-hole pairs.

It is to be noted that voltage was chosen for getting the highest and best in the different responsivity samples of Mg-doped and undoped at a wavelength of 365 and 385 nm as illustrated in Table3.

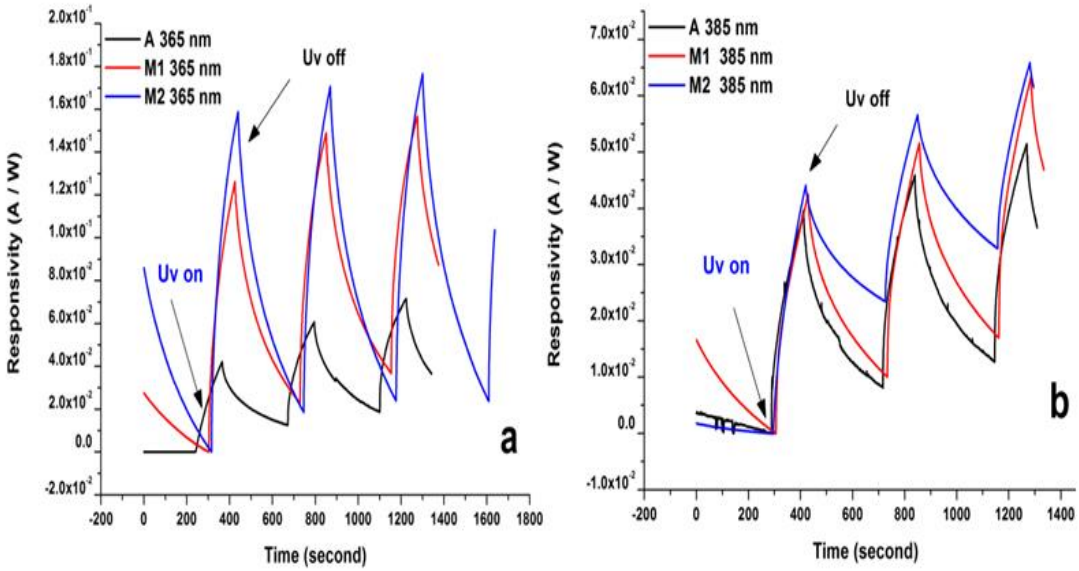


Figure 7: Responsivity with a time of MSM Mg-doped ZnO photodetectors are compared with MSM ZnO photodetector at a) UV 365nm b) UV 385nm

***Responsivity and quantum efficiency via wavelength***

The responsivity is defined as the generated photocurrent per unit power of incident light on the effective area of the photodetector and external quantum efficiency ($\eta$) is nothing but the number of electron-hole pairs generated due to the one absorbed a photon of energy hν. The responsivity and quantum efficiency of a device have been at 1V applied bias which calculated by equations 5 and 6 as a function of wavelength [27]

It is observed that the responsivity of devices Mg-doped ZnO samples M1and M2 shows a higher and shifted at low wavelength, these were a high responsivity in the UV region and prominently does not show a photo response to visible region, which is credited to the wide band gap energy of ZnO so that no charge carrier is excited at low energy visible photons.

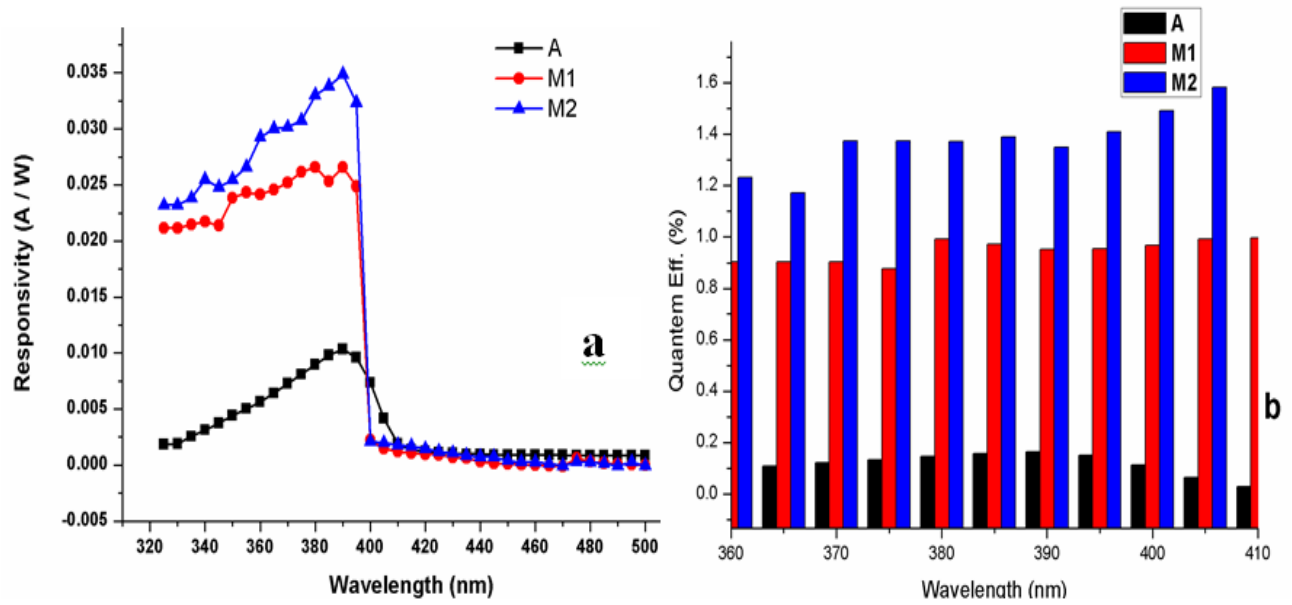


Figure 8: Responsivity and quantum efficiency as wavelength of MSM ZnO and MSM Mg-doped ZnO photodetectors

## Conclusions

In this work, the structural, optical and electrical properties were measured for pure and Mg-doped nanorods and nanotubes of ZnO were successfully synthesized by hydrothermal. The MSM UV has been fabricated based on a pure and Mg-doped ZnO thin film. The photoresponse properties under the action of UV were studied at room temperature, the performance of the photodetector can be improved with respect to the photocurrent, the contrast ratio, dark current, and detectivity. The MSM UV based on an Mg-doped ZnO has shown enhanced responsivity and quantum efficiency and others parameters under a voltage 10 V applied shown that Table4 that has compared to that pure ZnO at shifted low wavelength.

Table 4: Result parameters of devices are measured at 10 v applied biases of all samples

| sample | UV 365 nm | | | |
|---|---|---|---|---|
| | R A/W | $\eta$ | S % | D |
| **A** | 0.047 | 16.190 | 259.56383 | $7.23*10^{11}$ |
| **M1** | 0.1045 | 35.547 | 218.62517 | $9.81*10^{11}$ |
| **M2** | 0.118 | 40.051 | 224.44021 | $1.05*10^{12}$ |
| | **UV 385 nm** | | | |
| **A** | 0.036 | 11.8429 | 200.2726 | $5.58*10^{11}$ |
| **M1** | 0.0406 | 13.1947 | 85.5972 | $3.85*10^{11}$ |
| **M2** | 0.0426 | 13.7028 | 80.99512 | $3.8*10^{11}$ |

## References

[1] Z. R. Dai, Z. W. Pan, and Z. L. Wang, *Novel nanostructures of functional oxides synthesized by thermal evaporation.*

Advanced Functional Materials, 2003. 13(1): p. 9-24.

[2] M. S. Alam, U. Manzoor, M. Mujahid, and A. S. Bhatti1, *Highly Responsive UV Light Sensors Using Mg-Doped ZnO Nanoparticles.* Journal of Sensors, 2016.

[3] B.Santoshkumara, A. Biswasb, S. Kalyanaramana, R. Thangavelc, G.Udayabhanub, G. Annaduraid, and S. Velumanie, *Influence of defect luminescence and structural modification on the electrical properties of Magnesium Doped Zinc Oxide Nanorods.* Superlattices and Microstructures, 2017. **106**: p. 58-66.

[4] M. Zhao, X. Wanga, J. Cheng, L. Zhang, J. Jia, and X. Li, *Synthesis and ethanol sensing properties of Al-doped ZnO nanofibers.* Current Applied Physics, 2013. **13**(2): p. 403-407.

[5] N. Thaweesaeng, S. Supankit, W. Techidheera, and W. Pecharap, *Structure properties of as-synthesized Cu-doped ZnO nanopowder synthesized by co-precipitation method.* Energy Procedia, 2013. **34**: p. 682-688.

[6] A. Djurišić, A. Ng, and X. Chen, *ZnO nanostructures for optoelectronics: material properties and device applications.* Progress in quantum electronics, 2010. **34**(4): p. 191-259.

[7] H. T. Kim, T. P. Nguyen, C. Kim, and C. Park, *Formation mechanisms of pyrite (FeS2) nano-crystals synthesized by colloidal route in sulfur abundant environment.* Materials Chemistry and Physics, 2014. **148**(3): p. 1095-1098.

[8] J. X. Wang, X. W. Sun, Y. Yang, and L Vayssieres, *Hydrothermally grown oriented ZnO nanorod arrays for gas sensing applications.* Nanotechnology, 2006. **17**(19): p. 4995.

[9] J. Bao, M. A. Zimmler, F. Capasso, X. Wang, and Z. F. Ren, *Broadband ZnO single-nanowire light-emitting diode.* Nano letters, 2006. **6**(8): p. 1719-1722.

[10] L. Luo, Y. Zhang, S. Mao, and L. Lin, *Fabrication and characterization of ZnO nanowires based UV photodiodes.* Sensors and Actuators A: Physical, 2006. **127**(2): p. 201-206.

[11] Y. Lu, I. Dajani, and R. Knize, *ZnO nanorod arrays as pn heterojunction ultraviolet photodetectors.* Electronics Letters, 2006. **42**(22): p. 1309-1310.

[12] M. Fu, Y. Li, P. Lu, J. Liu, and F. Dong, *Sol–gel preparation and enhanced photocatalytic performance of Cu-doped ZnO nanoparticles.* Applied Surface Science, 2011. **258**(4): p. 1587-1591.

[13] L. Chow, O. Lupan, G. Chai, H. Khallaf, and L. K. Ono, *Synthesis and characterization of Cu-doped ZnO one-dimensional structures for miniaturized sensor applications with faster response.* Sensors and Actuators A: Physical, 2013. **189**: p. 399-408.

[14] O. Lupan, L. Chow, L. Ono, and B. Cuenya, *Synthesis and characterization of Ag-or Sb-doped ZnO nanorods by a facile hydrothermal route.* The Journal of Physical Chemistry C, 2010. **114**(29): p. 12401-12408.

[15] M. Habibi, and M. K. Sardashti, *Structure and morphology of nanostructured zinc oxide thin films prepared by dip-vs. spin-coating methods.* Journal of the Iranian Chemical Society, 2008. **5**(4): p. 603-609.

[16] A. Ohtomo, K. Tamura, M. Kawasaki, and T. Makino, *Room-temperature stimulated emission of excitons in ZnO/(Mg, Zn) O superlattices.* Applied Physics Letters, 2000. **77**(14): p. 2204-2206.

[17] E. Guidelli, O. Baffa, and D. Clarke, *Enhanced UV emission from silver/ZnO and gold/ZnO core-shell nanoparticles: photoluminescence, radioluminescence, and*

*optically stimulated luminescence.* Scientific reports, 2015. **5**: p. 14004.

[18] K. E. Knutsen, A. Galeckas, A. Zubiaga, and F. Tuomisto, *Zinc vacancy and oxygen interstitial in ZnO revealed by sequential annealing and electron irradiation.* Physical Review B, 2012. **86**(12): p. 121203.

[19] A. Janotti, and C. V. Walle, *Fundamentals of zinc oxide as a semiconductor.* Reports on progress in physics, 2009. **72**(12): p. 126501.

[20] H. Hsu, C. Wu, H. Cheng, and W. Hsieh, *Band gap engineering and stimulated emission of ZnMgO nanowires.* Applied Physics Letters, 2006. **89**(1): p. 013101.

[21] X. Wu, G. Siu, C. Fu, and H. Ong, *Photoluminescence and cathodoluminescence studies of stoichiometric and oxygen-deficient ZnO films.* Applied Physics Letters, 2001. **78**(16): p. 2285-2287.

[22] H. Wang, G. Wang, L. Jia, and C. Tang, *Polychromatic visible photoluminescence in porous ZnO nanotubes.* Journal of Physics D: Applied Physics, 2007. **40**(21): p. 6549.

[23] B. Sonawane, M. Bhole, and D. Patil, *Structural, optical and electrical properties of MgxZn1− xO ternary alloy films.* Materials Science in Semiconductor Processing, 2009. **12**(6): p. 212-216.

[24] C. L. Hsu, and S. J. Chang, *Doped ZnO 1D nanostructures: synthesis, properties, and photodetector application.* Small, 2014. **10**(22): p. 4562-4585.

[25] Y. Liu, C. Gorla, S Liang, N. Emanetoglu, Y. Lu, *Ultraviolet detectors based on epitaxial ZnO films grown by MOCVD.* Journal of Electronic Materials, 2000. **29**(1): p. 69-74.

[26] D. Zhang,and D. Brodie, *Photoresponse of polycrystalline ZnO films deposited by rf bias sputtering.* Thin Solid Films, 1995. **261**(1-2): p. 334-339.

[27] C. Chey, A. Masood, A. Riazanova, and X. Liu, *Synthesis of Fe-doped ZnO nanorods by rapid mixing hydrothermal method and its application for high performance UV photodetector.* Journal of Nanomaterials, 2014. p. 222.